

Article

Influence of Fluorine and Nitrogen Co-Doping on the Structural and Morphological Properties of Sol-Gel ZnO Films

Tatyana Ivanova ^{1,*}, Antoaneta Harizanova ¹, Tatyana Koutzarova ² , Benedicte Vertruyen ³ 
and Raphael Closset ³

¹ Central Laboratory of Solar Energy and New Energy Sources, Bulgarian Academy of Sciences, 1784 Sofia, Bulgaria

² Institute of Electronics, Bulgarian Academy of Sciences, 1784 Sofia, Bulgaria

³ GREENMAT, Institute of Chemistry B6, University of Liege, 4000 Liege, Belgium

* Correspondence: tativan@phys.bas.bg

Abstract: The structural, vibrational, optical and morphological properties of ZnO:N:F films, obtained by the sol-gel method, were investigated. The effect of single (fluorine, nitrogen) and F, N co-doping and thermal treatments (300–600 °C) on the properties of ZnO films was analyzed. X-ray Diffraction (XRD) revealed that ZnO:N:F films crystallized in a polycrystalline wurtzite structure. F and N incorporation changed lattice parameters, crystallite sizes, texture coefficients (TC) and residual stress. TC (002) of ZnO:N:F films increased with annealing, reaching 1.94 at 600 °C lower than the TC (002) of ZnO and ZnO:N films. The shifting of the characteristic absorption bands and/or the appearance of new IR lines were detected for ZnO:N:F samples. The highest transmittance (90.98%) in the visible spectral region was found for ZnO:F films. ZnO:N:F films possessed optical transparency up to 88.18% and their transmittance decreased at the higher annealings. The optical band gap (E_g) values of ZnO:N:F films were changed with fluorine and nitrogen concentrations. The formation of the wrinkle-like structures on the surface of ZnO and ZnO:N films was depicted in Field Emission Scanning Electron Microscopy (FESEM) images. The F, N dual doping modified ZnO morphology and suppressed wrinkle formation.

Keywords: sol-gel based coating; thin films; F:N dual doped ZnO; annealing temperatures; structure; optical properties



Citation: Ivanova, T.; Harizanova, A.; Koutzarova, T.; Vertruyen, B.; Closset, R. Influence of Fluorine and Nitrogen Co-Doping on the Structural and Morphological Properties of Sol-Gel ZnO Films. *Coatings* **2022**, *12*, 1874. <https://doi.org/10.3390/coatings12121874>

Academic Editors: Torsten Brezesinski and Ben Breitung

Received: 10 November 2022

Accepted: 30 November 2022

Published: 2 December 2022

Publisher's Note: MDPI stays neutral with regard to jurisdictional claims in published maps and institutional affiliations.



Copyright: © 2022 by the authors. Licensee MDPI, Basel, Switzerland. This article is an open access article distributed under the terms and conditions of the Creative Commons Attribution (CC BY) license (<https://creativecommons.org/licenses/by/4.0/>).

1. Introduction

Zinc oxide (ZnO) is considered as one of the most promising materials among metal oxide semiconductors due to its fascinating physical and chemical properties [1]. ZnO possesses wide band gap ($E_g = 3.37$ eV at room temperature), large exciton binding energy (60 meV), high transparency in the visible spectral range, low cost, non-toxicity, and advantages in technology and resistance to radiation damage [2]. ZnO materials have gained great research interest because of their photocatalytic [3], piezoelectric [4], antibacterial [5], and electrical [6] properties. ZnO is efficiently applied in optoelectronic and nanoelectronic devices [1,7], surface acoustic wave devices, gas sensors and as antireflection coatings and windows in solar cells and transparent electrodes [8,9]. Meanwhile, non-toxicity, biocompatibility, chemical stability and photochemical properties make ZnO desirable candidates for drug delivery and photo-catalytic uses [10,11].

The structural, optical and electrical properties of ZnO can be modified and improved by metal and nonmetal doping. For example, it has been reported that Ga, In, and Mg dopants lead to enhanced transparency, tuning of the optical band gap and low resistivity [12]. Doped ZnO films become a promising alternative for transparent conductive oxide [12] and for new energy low-E coating [13].

The fluorine incorporation possesses several advantages over other doping elements due to its low cost and abundance. Also, it is known that fluorine ionic radius (1.36 Å)

allows F to substitute in oxygen sites (as oxygen ionic radius is 1.40 Å) or in oxygen vacancies in ZnO structures [14]. The F doping can induce the improvement of conductivity, optical properties and morphological change in ZnO films [14,15]. The photocatalytic antibacterial activities in the visible light of nanocrystalline ZnO photocatalysts have been achieved through fluorine doping [16]. It is reported that incorporating F as an anion in ZnO results in better performance of the perovskite-based solar cells [17].

The photovoltaic parameters and the light-harvesting capacity of the whole solar cell are enhanced due to the great crystallite sizes, the low oxygen-related defect state density, the good hydrophobic surface, and the high conductivity of ZnO:F electron transport layers [17].

Nitrogen is also recognized as an appropriate dopant in the ZnO lattice to substitute oxygen since it has a similar atomic radius and electronegativity as O [18]. Nitrogen inclusion is an efficient approach for obtaining p-type ZnO [19]. ZnO:N materials have shown very useful and interesting features such as ferromagnetism, with no doping of access magnetic ions [20] and excellent photo responsivity [21].

There are various deposition methods to fabricate ZnO based films, including hydrothermal synthesis [22], spray pyrolysis [23], chemical vapor deposition [24], magnetron sputtering [25], pulsed laser deposition [26] and electrodeposition [27]. Among these, the sol-gel technology is advantageous due to its low operation cost, non-vacuum requirements, non-expensive equipment, large area film deposition, compositional modifications, precise microstructural and chemical control, reproducibility and the possibility of engineering the film properties. The sol-gel method is regarded as one of the most conventional methods to produce different materials owing to its simplicity, lack of requirement for special equipment, and diversity of thin films and nanoparticles [28]. Furthermore, the controllability of the dopant concentration and homogeneous composition distribution is easy using the sol-gel method [29]. The spin coating method is a scalable technique and has been widely used in the coating industry to prepare high-quality ZnO thin films [1].

Thus, doping of impurities is a well-known and efficient method for tuning the properties of thin-film structures. In this regard, the doping of elements into the host lattice has become routine in many cases, and this thought process has paved the way for the co-doping of elements into the host lattice [30]. The aim of this work is the preparation of ZnO:N:F thin films and to study the influence of two dopants on the structural, vibrational and optical properties of ZnO. The undoped ZnO, single N, F doped and co-doped ZnO films are deposited by a facile sol-gel method on Si and quartz substrates. The effect of the annealing temperatures on the crystal structure, the texture coefficients, the lattice parameters, IR absorption bands, the film transparency and the surface morphology of ZnO:N:F films is investigated using XRD analysis, FESEM observation, FTIR spectroscopy and UV-VIS spectroscopy, respectively.

2. Materials and Methods

2.1. Thin Film Preparation

The technological sequence of the synthesis steps of sols for depositing ZnO, doped ZnO and ZnO:N:F films and the thin film preparation is schematically illustrated in Figure 1. The synthesis of 0.4 M sol solution for ZnO deposition was previously reported [31]. Zinc acetate dihydrate $\text{Zn}(\text{CH}_3\text{COO})_2 \cdot 2\text{H}_2\text{O}$ (Riedel de Haen, Hannover, Germany) was used as Zn precursor and dissolved in absolute ethanol (Merck KgaA Darmstadt, Germany, absolute for analysis). The complexing agent was monoethanolamine (MEA, Fluka AG, Buchs, Switzerland, 98%) with MEA/Zn molar ratio = 1 [31]. The fluorine precursor used was ammonium fluoride (NH_4F , Fluka AG, Buchs, Switzerland). The mixed sols (Zn-F) were prepared by adding 0.1 and 0.5 wt% NH_4F into the appropriate Zn sol volume. The corresponding obtained sols and thin films, deposited from these sols are labeled as ZnO:F 0.1 and ZnO:F 0.5 [32]. The Zn-N sol was derived by adding 1 wt% ammonium acetate ($\text{CH}_3\text{COONH}_4$, Sigma-Aldrich Chemie GmbH, Taufkirchen, Germany) into Zn solution [33]. The sols were stirred on a magnetic stirrer type (ARE, Velp Scientifica s.r.l.,

Usmate, Italy) at 50 °C/2 h, then ultrasonically (ultrasonic cleaner, UST 2.8-100, Siel Ltd., Gabrovo, Bulgaria) treated at 40 °C/3 h. The obtained sols were clear, transparent, and without precipitation.

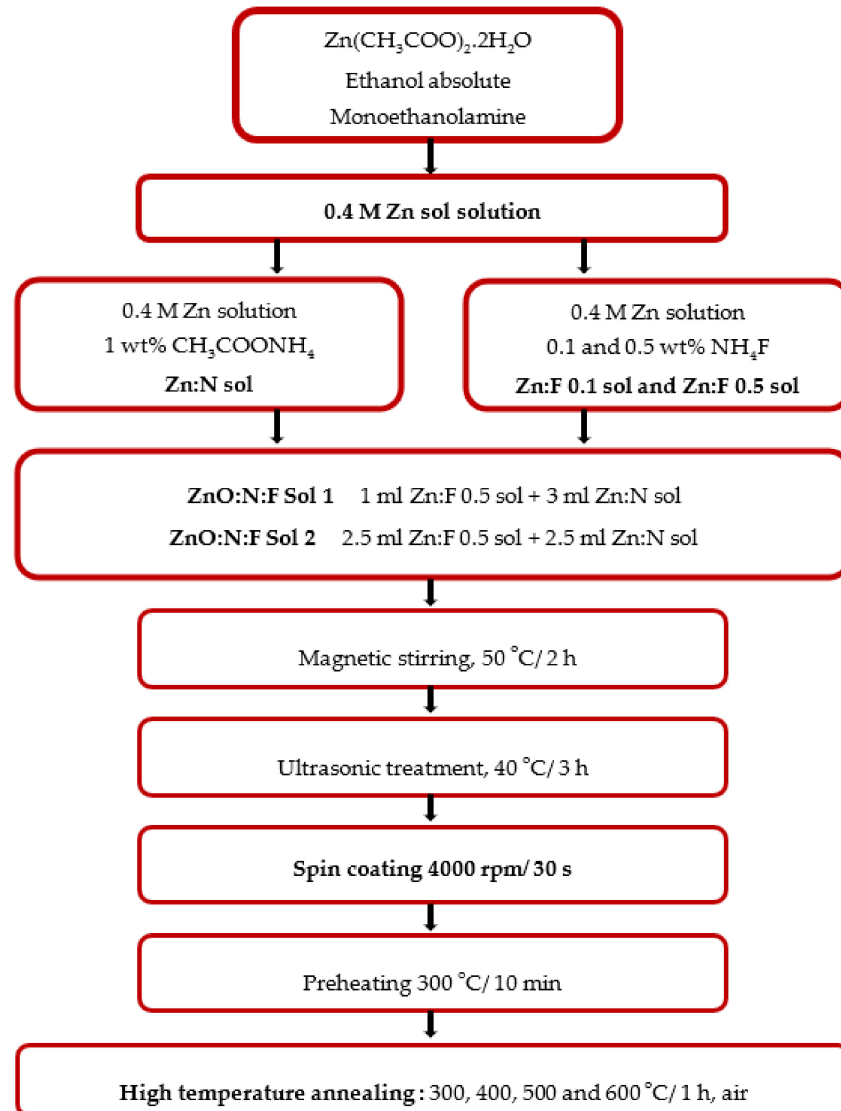


Figure 1. Schema of sol solution synthesis and thin film deposition.

ZnO, ZnO:N, ZnO:F and ZnO:N:F films were deposited by spin coating (Spin coater P 6708, PI-KEM Limited, Staffordshire, UK) at 4000 rpm/30 sec on preliminary cleaned substrates, followed by preheating at 300 °C/10 min. Si wafers (FZ, p-type, resistivity 4.5–7.5 Ω, orientation <100>) were applied for structural and surface morphology research and UV graded quartz glass substrates (thickness 1 mm ± 0.1) were used for optical characterization.

The coating and preheating procedures were repeated five times. The obtained films were finally annealed at the temperatures of 300, 400, 500 and 600 °C for 1 h in air in a chamber furnace (Tokmet-TK Ltd., Varna, Bulgaria). The heating rates were controlled and kept constant at 10 °C/min.

2.2. Thin Film Characterization

X-Ray diffraction patterns were recorded by an XRD diffractometer Bruker D8 (Bruker AXS GmbH, Karlsruhe, Germany) using a Cu anode ($\lambda_{K\alpha} = 1.54056 \text{ \AA}$), a grazing angle of 2°, and a step time of 8 s. FTIR spectra were taken by Shimadzu Spectrophotometer IRPrestige-

21 (resolution of 4 cm^{-1} , Shimadzu, Kyoto, Japan) in the spectral range $350\text{--}4000\text{ cm}^{-1}$ using bare Si wafer as background.

Optical transmittance and reflectance spectra were carried out by UV-VIS-NIR Shimadzu 3600 double-beam spectrophotometer (with resolution 0.1 nm , Shimadzu, Kyoto, Japan) in the spectral region of $240\text{--}1800\text{ nm}$. The transmittance was measured against air and the reflectance was measured by using the specular reflectance attachment (5° incidence angle) and Al coated mirror as reference.

The film morphology of the studied ZnO based films were investigated by FESEM-Field Emission scanning electron microscopy (Philips XL 30FEG-ESEM, FEI, Thermo Fisher Scientific, Waltham, USA). The investigated samples had been coated with gold before microscopic observation. Different magnifications were applied.

3. Results and Discussions

3.1. XRD Analysis

Figure 2 presents the XRD patterns of sol-gel (N, F) co-doped ZnO films, treated at temperatures from 300 to $600\text{ }^\circ\text{C}$. The recorded diffraction peaks are indexed to the hexagonal wurtzite structure of zinc oxide with space group $P63mc$ (186) (JCPDS card 01-070-8070).

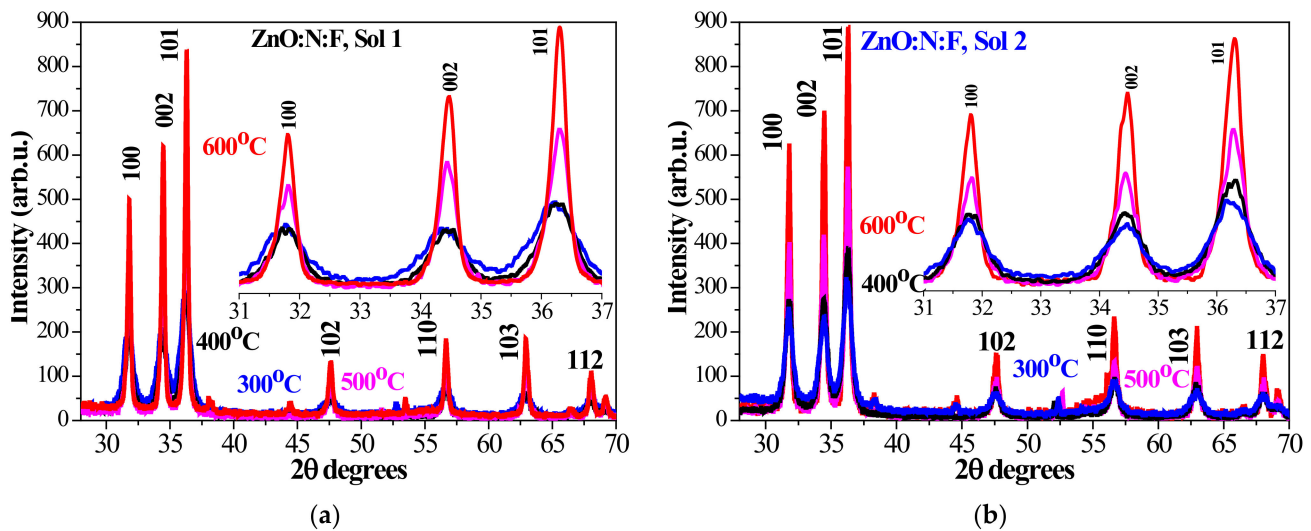


Figure 2. XRD patterns of (a) ZnO:N:F films (Sol 1), (b) ZnO:N:F films (Sol 2), treated at 300 , 400 , 500 and $600\text{ }^\circ\text{C}$. The inset figures present the enlarged XRD patterns in 2θ range = $31\text{--}37^\circ$.

The sol-gel undoped ZnO films are polycrystalline and the film crystallization increases with the annealing temperatures [31]. Our previous investigation of sol-gel ZnO:F films (after annealing at $500\text{--}800\text{ }^\circ\text{C}$) [32] confirms that fluorine introduction does not induce any change of wurtzite structure. Nitrogen doping results in an improved crystallinity compared to ZnO film, sustaining the wurtzite phase [33]. It is worth noting that the F, N co-doped ZnO films exhibit a polycrystalline structure with stronger lines than those of undoped ZnO.

The weaker diffractions at 38.3° , 44.5° and 53.2° are detected for ZnO:N:F films and for ZnO (the two lower angle lines). They can be probably attributed to ZnO_2 phase [34] or to Zn [35]. No secondary phases corresponding to F or N are detected. As can be seen from Figure 2 (the inserted enlarged patterns), XRD (100), (002) and (101) lines become stronger and narrower with increasing the annealing temperatures, indicating that the crystallites grow bigger. XRD analysis confirms that the crystallinity of the films is significantly improved with high temperature treatments.

Figure 3a,b, shows the shifting of the three strongest diffraction peaks induced by different doping: ZnO:N, ZnO:F 0.1, ZnO:F 0.5 and ZnO:N:F films (Sol 1 and Sol 2), after annealing at 500 and $600\text{ }^\circ\text{C}$, respectively. Figure 3c presents the shifting of 002 line (the

variation from ZnO line position, $\Delta 2\theta$ degrees = 2θ (ZnO) - 2θ (doped ZnO)) of ZnO:N:F films as a function of the annealing temperature. It can be seen that co-doping results in 002 line shifting to smaller angles. The smallest shift is detected after thermal treatment at 400 °C. It has been affirmed that the (002) peak is shifted to the higher angles for ZnO:N films [31], indicating that nitrogen is successfully incorporated into zinc oxide lattice and that N can partially substitute oxygen [36]. There is a shifting for ZnO:F 0.1 films as when increasing the fluorine concentration (ZnO:F 0.5), the shift is more distinct. The peak shifting is evidence of the incorporation of nitrogen and fluorine into the ZnO lattice.

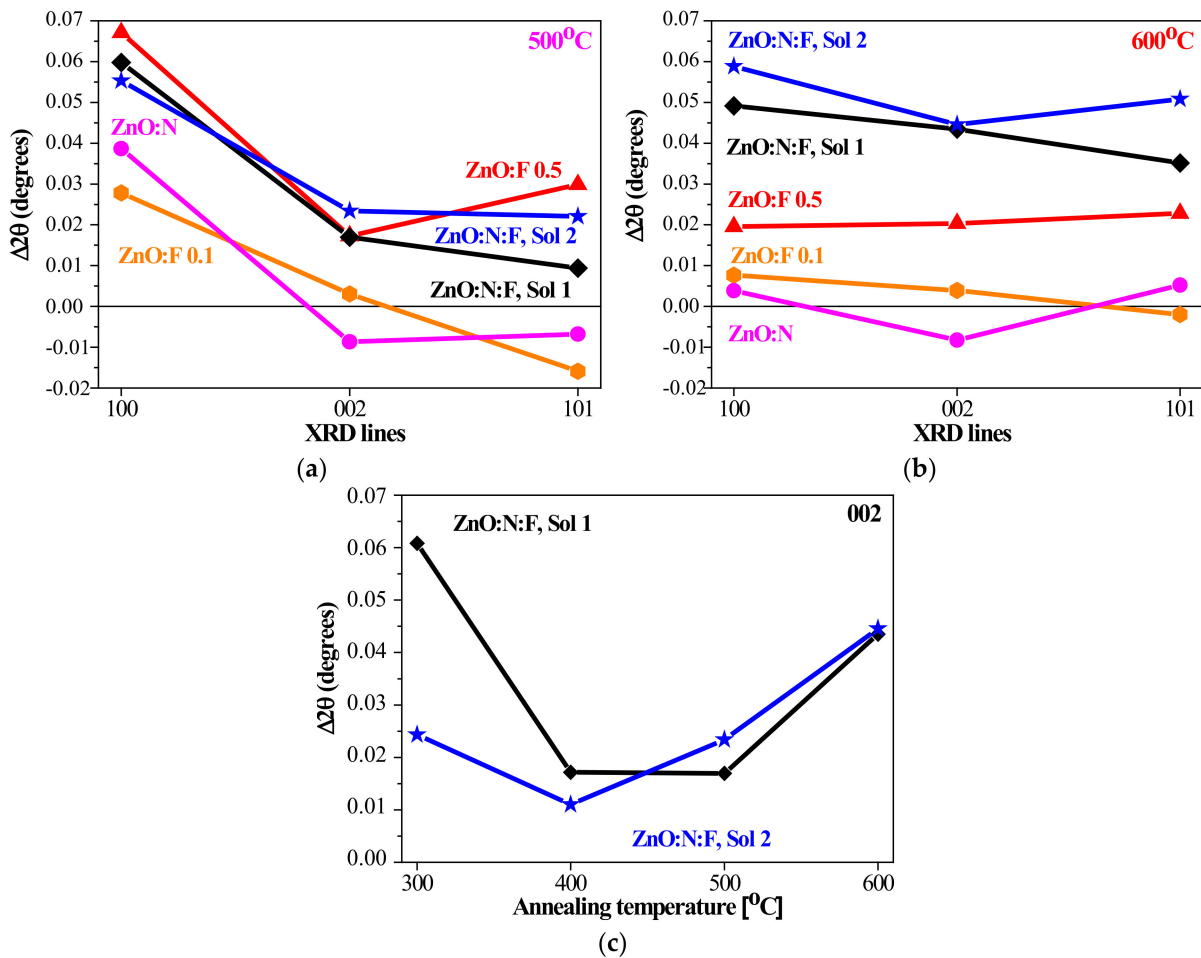


Figure 3. The shifting ($\Delta 2\theta$) of XRD (100), (002) and (101) lines for ZnO based films, annealed at (a) 500 °C and at (b) 600 °C is given and (c) presents the shifting of (002) peak for ZnO:N:F films as a function of the annealing temperature.

The crystallite sizes are calculated using Scherrer’s equation, based on the broadening of the five diffraction lines ((100), (002), (101), (102) and (110)), and the obtained average values are presented in Table 1. The crystallites grow bigger with the increase in the annealing temperature for the all studied films. It is noted that the greatest crystallites are determined for ZnO:F films. ZnO:N films also crystallize with growing greater crystallites. It has been reported that the ion implantation of nitrogen in ZnO can change stoichiometry (due to N replacing O sites in ZnO structure) and respectively, this provokes expansion of the crystallite sizes [37].

Table 1. Crystallite sizes, lattice parameters, c and a , c/a ratio and residual stress σ_{film} are determined from XRD patterns of ZnO based films.

Material		300 °C	400 °C	500 °C	600 °C
ZnO	Crystallite size [nm]	9.91	12.17	25.66	29.96
	a [Å]	3.241	3.246	3.244	3.244
	c [Å]	5.199	5.200	5.200	5.199
	c/a ratio	1.60413	1.60197	1.60296	1.60265
	σ_{film} [GPa]	26.41	21.94	21.94	26.41
ZnO:F 0.1	Crystallite size [nm]			33.30	35.61
	a [Å]			3.244	3.244
	c [Å]			5.200	5.196
	c/a ratio			1.60296	1.60173
	σ_{film} [GPa]			21.94	39.84
ZnO:F 0.5	Crystallite size [nm]			26.92	38.63
	a [Å]			3.247	3.244
	c [Å]			5.199	5.199
	c/a ratio			1.60117	1.60265
	σ_{film} [GPa]			26.41	26.41
ZnO:N	Crystallite size [nm]	10.65	15.43	27.00	31.84
	a [Å]	3.266	3.244	3.245	3.243
	c [Å]	5.209	5.203	5.196	5.194
	c/a ratio	1.59492	1.60388	1.60123	1.60160
	σ_{film} [GPa]	−18.35	8.50	39.84	48.79
ZnO:N:F, Sol 1	Crystallite size [nm]	9.21	12.39	20.56	27.98
	a [Å]	3.248	3.245	3.242	3.245
	c [Å]	5.200	5.201	5.197	5.198
	c/a ratio	1.60099	1.60277	1.60302	1.60185
	σ_{film} [GPa]	21.94	17.46	35.36	30.89
ZnO:N:F, Sol 2	Crystallite size [nm]	11.34	12.64	17.07	24.79
	a [Å]	3.247	3.244	3.245	3.247
	c [Å]	5.202	5.199	5.198	5.196
	c/a ratio	1.60209	1.60265	1.60185	1.60025
	σ_{film} [GPa]	12.98	26.41	30.89	39.84
ZnO, wurtzite * $a = 3.2489$ Å; $c = 5.2049$ Å; c/a ratio = 1.60205					

* JCPDS card 01-070-8070.

It can be concluded that single doping with nitrogen and fluorine promotes the crystallites growth. This effect can be related to the change in the crystal lattice as F and N dopants can partially substitute oxygen in ZnO. In the case of N, F co-doped films, the crystallite values are closer or slightly higher (ZnO:N:F films (Sol 2)) to the crystallite sizes of ZnO after annealings at 300 and 400 °C. The high thermal treatments (500 and 600 °C) lead to smaller crystallites of ZnO:N:F films compared to those of ZnO, ZnO:F and ZnO:N. The co-doping with N and F inhibits the crystallite growth resulting in smaller crystallite sizes, nevertheless single doping either with nitrogen or with fluorine leads to the formation of bigger crystallites. This result suggests that the co-doping might cause the formation of more defects than single F and N doping. The lattice parameters are estimated from XRD data and the obtained values are presented in Table 1. They are dependent on the doping, co-doping and on the annealing temperatures. The lattice parameter c of undoped ZnO films is slightly changed with annealing. ZnO:N films show considerable reduction of the c -axis with increasing the annealing temperatures from 5.209 Å (300 °C) to 5.194 Å (600 °C). ZnO:F 0.5 films have closer values to undoped ZnO. The c parameter of ZnO:F 0.1 film, treated at 600 °C is 5.196 Å. ZnO:N:F films, deposited from Sol 1 show no clear trend. ZnO:N:F films, from Sol 2 reveal diminishing of c from 5.202 to 5.196 Å with increasing the annealing temperatures. The lattice parameter a varies with the thermal treatments. It is

well known that the changes in the lattice parameters are induced by impurities, lattice defects, vacancies, deposition conditions and the concentration of native imperfections in thin films.

The c/a ratio is determined (see Table 1). It is accepted that in doped ZnO, the wurtzite structure diverges from the ideal arrangement by changing the c/a ratio [38]. The ideal c/a ratio is 1.633 [39]. It is seen that the c/a ratio values are greatly influenced by the annealing temperature and the dopants. The ZnO based films treated at 300 °C reveal a decrease of c/a ratio with doping, especially for ZnO:N films. The annealings at the higher temperature result in smaller differences in c/a ratio values. The comparison of undoped ZnO and co-doped ZnO films reveals that bigger deviations of the c/a ratio are found after annealing at 300 and 600 °C.

The film residual stress, σ_{film} values are estimated for additional structural information of the studied films using XRD data (see Table 1). The c -axis strain (ϵ_{zz}) values have been calculated by using the following formula [40]:

$$\epsilon_{zz} = \frac{c - c_0}{c_0} \times 100\% \quad (1)$$

where c is the calculated lattice parameter from X-ray diffraction data and $c_0 = 5.2049 \text{ \AA}$ is the unstrained lattice parameter of ZnO.

For hexagonal crystals, the residual stress, σ_{film} , in the plane of the film can be calculated [40]:

$$\sigma_{film} = \frac{2c_{13}^2 - c_{33}(c_{11} + c_{12})}{2c_{13}} \times \epsilon_{zz} \quad (2)$$

where ϵ_{zz} is the determined c -axis strain and c_{ij} depicts the elastic stiffness constants ($c_{11} = 208.8 \text{ GPa}$, $c_{33} = 213.8 \text{ GPa}$, $c_{12} = 119.7 \text{ GPa}$ and $c_{13} = 104.2 \text{ GPa}$). Thus, the residual stress can be estimated from [40]:

$$\sigma_{film} = -233 \times \epsilon_{zz} \text{ (GPa)} \quad (3)$$

The estimated values of σ_{film} from Equation (3) are presented in Table 1. The total stress of thin film consisted of (i) intrinsic stress (due to impurities, defects and lattice distortions); and (ii) extrinsic stress (lattice mismatch and thermal expansion coefficient difference between film and substrate used). In our case, the used substrates (Si wafers), the technological parameters (spinning rate, preheating and annealing procedures, number of layers) of ZnO and doped ZnO film depositions are the same. Therefore, the stress variation is supposed to be determined primarily by the intrinsic stress. The negative sign of the stress values denotes biaxial compressive stress and the positive sign indicates tensile stress. The residual stresses in thin film are affected by the microstructure, recrystallization, microstructural variations at the film/substrate interface and/or other phase transformations. The intrinsic stress could generate defects like twins, precipitates, disoriented grains, grain boundaries and micro cracks [37].

The sol-gel ZnO:N films show a compressive stress after the low temperature treatment at 300 °C. After the increase of the annealing temperatures the stress turns into tensile. The undoped ZnO films possess tensile stress values in the range of 21.9–26.4 GPa. ZnO:F 0.1 films has tensile stress, which becomes greater with annealing. On the other hand, ZnO:F 0.5 films show tensile stress of 26.4 GPa, independent of the thermal treatments (500 and 600 °C). The stress of F, N co-doped ZnO films is tensile. The tensile stress of the co-doped films, obtained from Sol 1, varies from 17.5 to 35.4 GPa. Meanwhile, for ZnO:N:F films, Sol 2 display an increase of the tensile stress values with the annealing temperatures from 12.9 GPa (300 °C) to 39.9 GPa (600 °C). ZnO films are found to manifest the lower stress after the annealing at 500 and 600 °C. Nitrogen incorporation provokes the higher stress variation with the change of compressive stress (300 °C) to tensile (400–600 °C) as well as the greatest values of tensile stress, 39.8 and 48.8 GPa for 500 °C and 600 °C films,

respectively. On the other hand, ZnO:N films also reveal the lowest stress, 8.5 GPa, when the films are treated at 400 °C.

The degrees of the preferential orientation along the three crystalplanes 100, 002 and 101 of undoped, N doped, F doped and (N, F) co-doped ZnO films are estimated by calculating the corresponding texture coefficients (TC (hkl)), The obtained results are presented in Figure 4. The texture coefficients (TC) are determined using the JCPDS card 01-070-8070, considering the standard intensities for (100), (002), (101), (102), (110), (103), and (112) planes, respectively. A sample with randomly oriented crystallites yields TC (hkl) = 1 or lower, while the larger TC (hkl) is the larger abundance of crystallites orientated in the corresponding (hkl) direction [41]. Furthermore, TC values between 0.00 and 1.00 indicate a lack of grains orientated in the certain direction. Meanwhile, the greater deviation from unity is a sign for the higher preferred orientation of the studied film.

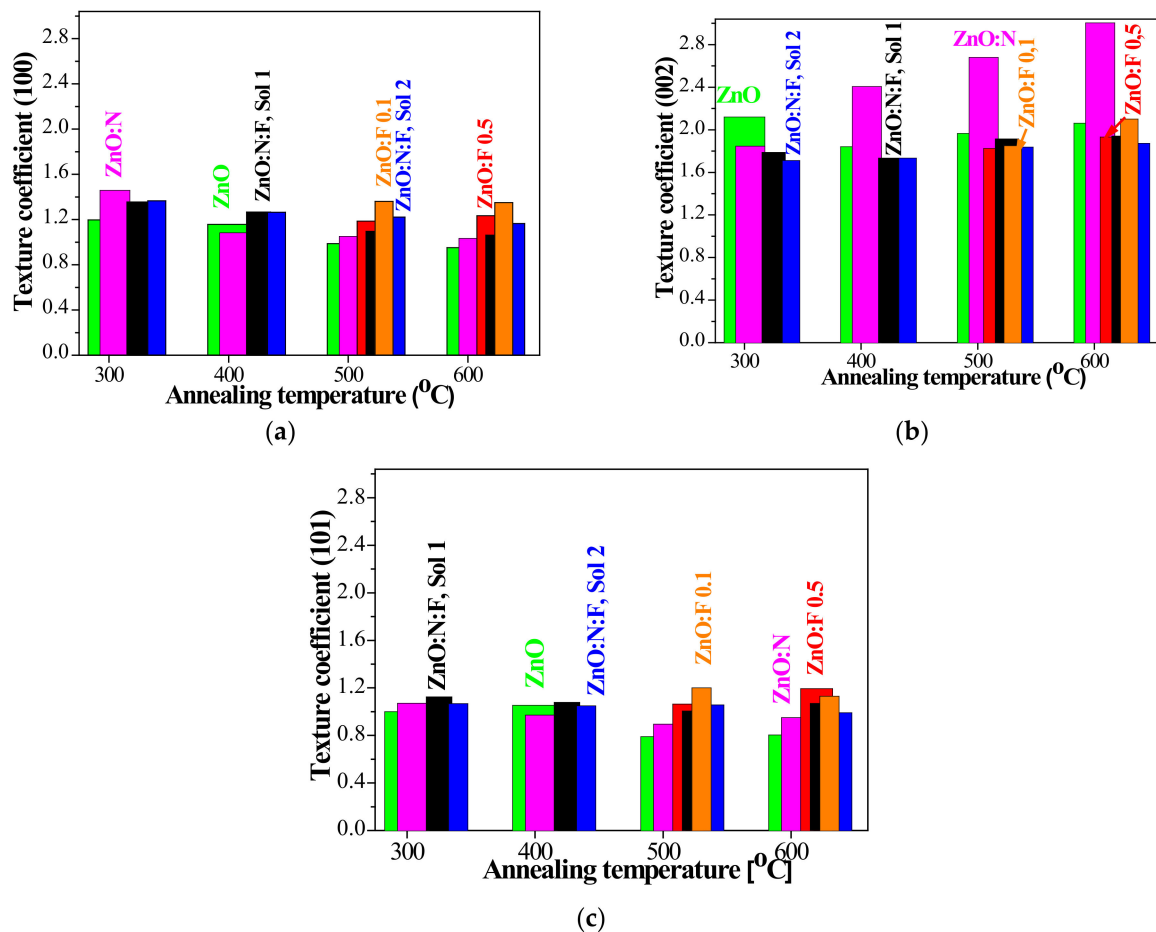


Figure 4. Texture coefficients of (a) (100), (b) (002) and (c) (101) peaks of ZnO based films as a function of the annealing temperatures.

Figure 4 shows that the highest TC values in (002) the plane are observed for ZnO:N films after annealing above 300 °C as the value reaches TC (002) = 3.0 (600 °C), suggesting that the incorporation of nitrogen atoms causes preferable *c*-axis growth. Similar results of increased preferred orientation are also reported due to the co-doping effect with N and Cu in ZnO lattice [42]. The texture coefficient of 002 plane of ZnO is changed (1.84–2.12) with the thermal treatments along with lowering of the values of TC (100) and TC (101). The texture coefficient of the crystal plane 002 for ZnO:N:F films is slightly increased with annealing temperatures, and it is varied from 1.79 to 1.94 for the films, deposited from Sol 1 and from 1.71 to 1.87 for Sol 2 samples, respectively. ZnO films show higher TC (002) values than ZnO:N:F films.

ZnO:N:F films possess TC (100) values higher than the corresponding values for ZnO films (for all annealing temperatures) and for ZnO:N films (above 300 °C). ZnO:N:F films have lower values of TC (002) than those of undoped ZnO and ZnO:N films. The TC (101) of ZnO:N:F films is higher compared to the TC (101) of ZnO and ZnO:N films. Texture coefficients are affected by the doping element and the annealing temperatures.

XRD analysis shows that ZnO and co-doped ZnO films are polycrystalline and nanostructured. Their crystallization improves with increasing the annealing temperatures. The co-doping with F and N in ZnO reflects on lattice parameters, residual stress, texture coefficients. The highest deviation from the undoped zinc oxide films are found for ZnO:N films. The crystallite growth is inhibited and the preferential orientation along crystal planes is modified due to fluorine and nitrogen incorporation in the ZnO structure.

3.2. FTIR Spectroscopy

The vibrational properties of the sol-gel films are studied by FTIR spectroscopy, which is employed as a supplementary tool to XRD analysis. It is known that the shapes and the intensities of IR absorption bands are influenced by crystallization degree, chemical composition, the presence of impurities, stress, film morphology, crystallite sizes and forms [43]. The doping in the ZnO lattice can cause the shifting and changing of characteristic IR lines and/or the appearance of new bands.

Figure 5 shows the FTIR spectra of sol-gel ZnO:N:F films, deposited from Sol 1 (a), Sol 2 (b) and the comparison of ZnO and doped ZnO films treated at 600 °C (Figure 5c,d). FTIR spectra of ZnO:N:F films display changes in the main absorption bands with increasing the annealing temperature, as the bands are getting stronger and narrower. This indicates improved crystallization, confirming the XRD study.

The absorption features observed in FTIR spectra of ZnO:N:F films (Sol 1) are at 1015 cm^{-1} , broad band at 840–980 cm^{-1} , weak lines at 673, 525, and 471 cm^{-1} with the main line centered at 390–405 cm^{-1} (shifting with raising the annealing temperatures is detected). The observed IR lines are related to Zn-O vibrations [44,45]. For ZnO:N:F films (Sol 2), the same bands are seen with some new features. The FTIR spectrum of the 300 °C annealed sample shows a splitting of the main band into two lines at 399 and 419 cm^{-1} . After 500 and 600 °C, ZnO:N:F films (Sol 2) manifest additional IR peaks at 368 and 379 (600 °C) cm^{-1} . The broad band at 840–980 cm^{-1} can be associated with several contributions, including the vibrational mode at 886 cm^{-1} (related to substitutional hydrogen at the oxygen site bound to the lattice Zn site, as a result of nitrogen incorporation) [46], and absorptions due to the formation of tetrahedral coordination of Zn and/or to C-O bonding [47,48].

An FTIR spectra comparison of ZnO, ZnO:N, ZnO:F 0.5 and ZnO:N:F films, annealed at 600 °C is presented in Figure 5c,d. ZnO films reveal very weak lines at 667–680 cm^{-1} , a broad absorption band at 617 cm^{-1} , and clear IR lines at 522, 420 and 395 cm^{-1} . All these lines are related to Zn-O stretching modes [44,49] as the absorption at 520 cm^{-1} is reported to be a sign of a Zn-O bond in a wurtzite structure [49]. The main absorption lines (located at 395–399 cm^{-1}) become stronger and sharper after high temperature annealing. These bands are also associated with Zn-O stretching vibrations, characteristic for wurtzite ZnO [49]. FTIR spectrum of ZnO:F films, treated at 600 °C shows that the fluorine doping changes shapes, positions of Zn-O bonds and the appearance of new peaks. The main absorption bands are situated around 395 cm^{-1} along with weaker band near 520 cm^{-1} , assigned to phonon modes of wurtzite [45]. The weaker bands at 678 and 478 cm^{-1} can also be assigned to the stretching Zn-O vibrations. The nitrogen doping in ZnO is reported to be manifested by the modification of the absorption features, related to hydroxyl group vibrations, C-H, O-H and N-H bonds [50]. The spectra of ZnO:N and ZnO:N:F films show weak IR bands at 3110 and 3200 cm^{-1} , and stronger absorption bands above 3400 cm^{-1} (3630, 3750 and 3855 cm^{-1}), related to hydroxyl group vibrations. These bands are absent for undoped ZnO and ZnO:F films. The other great difference in FTIR spectra is the absorptions in the spectral range 1050–1900 cm^{-1} , where ZnO and ZnO:F films have no IR features. The IR lines, observed for ZnO:N and (N, F) doped ZnO films, deposited from

Sol 1 and 2 (all annealing temperatures) at 2960 and 2850 cm^{-1} are due to C-H stretching modes. The line at 2340 cm^{-1} is assigned to atmospheric CO_2 (seen in all spectra) [51]. The main absorption bands of ZnO:N and ZnO:N:F (Sol 2) films manifest complicated shapes and splitting. Similar splitting of the IR band is reported as the influence of N doping in ZnO [46], and it can be due to the variation of the oxygen defect density [46]. FTIR analysis reveals that nitrogen doping significantly affects the absorption features of ZnO:N and ZnO:N:F films. The absorption features suggest that nitrogen is successfully incorporated in the ZnO structure.

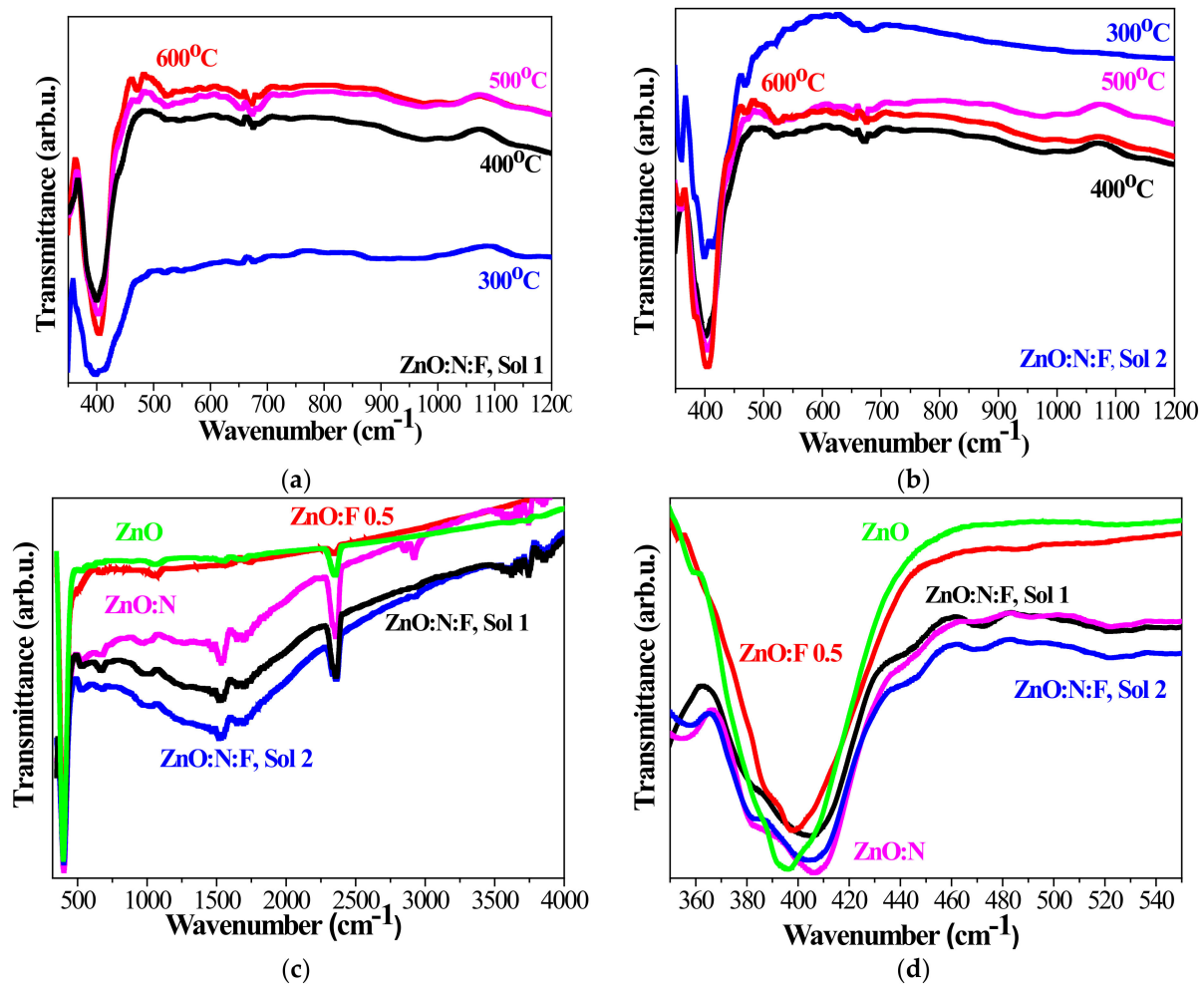


Figure 5. FTIR spectra of ZnO:N:F films, deposited from (a) Sol 1 and (b) Sol 2 and annealed at 300, 400, 500 and 600 °C. Figure (c) presents the FTIR spectra of ZnO, ZnO:N, ZnO:F and ZnO:N:F films, treated at 600 °C in the spectral range 350–4000 cm^{-1} and (d) the enlarged spectra in 350–550 cm^{-1} .

Figure 5d shows the modification of the strongest IR line with doping of the studied ZnO films after high temperature treatment. The shifting and widening of these bands with nitrogen, fluorine and N-F co-doping can be seen. The IR peak of ZnO film is broad and centered at 395 cm^{-1} , N doping results in moving the main band to 407 cm^{-1} with a shoulder at 382 cm^{-1} . ZnO:F film possesses its broad band at 398 cm^{-1} with clear contribution at 388 cm^{-1} . The co-doping ZnO films exhibit IR absorption at 405 cm^{-1} (ZnO:N:F, Sol 1) and at 405, 382 and 358 cm^{-1} . Obvious changes occur in the FTIR transmittance spectra of ZnO:N:F films as the dual incorporation of N and F manifest complex effects, but FTIR data confirm XRD conclusions that the sol-gel films maintain the wurtzite ZnO structure.

3.3. Optical Characterization

The transmittance and reflectance spectra of the sol-gel ZnO:N:F films, treated at different annealing temperatures, are presented in Figure 6. It is seen that ZnO:N:F films, obtained from Sol 1 (Figure 6a), are transparent (approaching 87% in the visible spectrum of 400 °C annealed film) and the transmittance is worsening with the higher annealing, especially after 600 °C, where the transparency is roughly 83%.

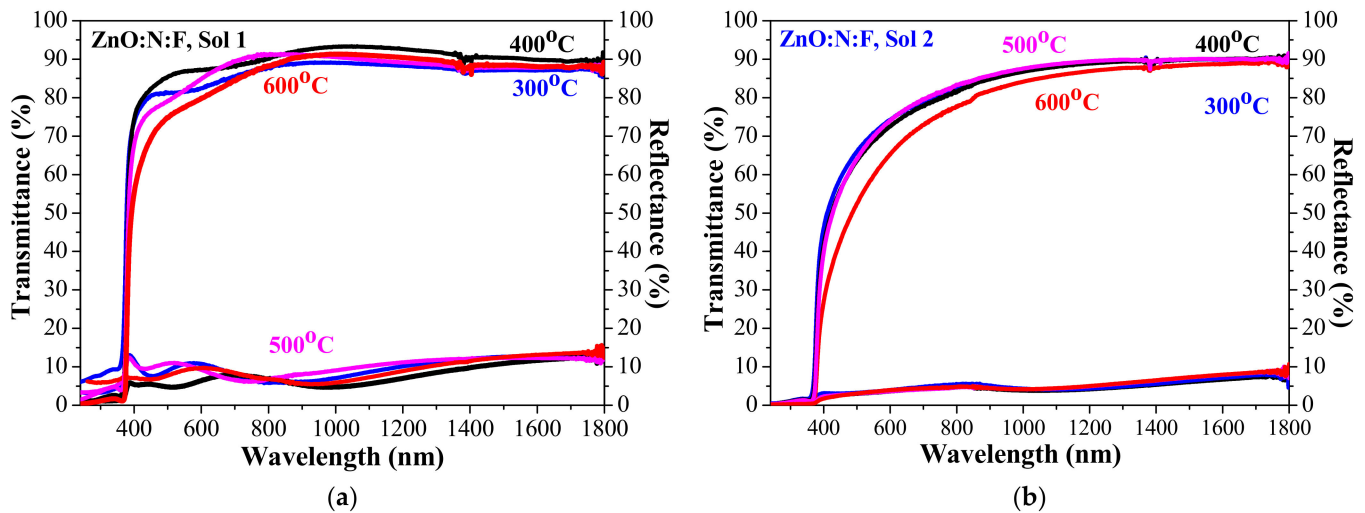


Figure 6. Transmittance and reflectance spectra of ZnO:N:F films, deposited from (a) Sol 1 and (b) Sol 2, thermally treated at different annealing temperatures.

It must be pointed out that the spectra are measured against air and that the films are deposited on quartz substrates (the used quartz substrate possesses 93% transparency in the visible spectral range). The film reflectance is below 15%.

The spectra of ZnO:N:F films, deposited from Sol 2 (Figure 6b), reveal almost no change in the recorded spectral range for the annealing temperatures of 300–500 °C. The transmittance is diminished after thermal treatment at 600 °C from 76% to 66%. These films have lower transparency in the visible spectral range compared to ZnO:N:F films, obtained from Sol 1. Undoped ZnO films also reduce their transparency with higher temperature annealing [31]. This can be provoked by greater crystallites, and respectively higher scattering from the film surface.

Figure 7 expresses the influence of fluorine doping and F, N co-doping on the transmittance spectra of the films treated at 500 °C (Figure 7a) and 600 °C (Figure 7b). A peak in the UV spectral region can be seen at 340 nm, which is related to the exciton formation [52]. This feature is observed for ZnO:N:F films deposited from Sol 1 and Sol 2. The effect is more clearly expressed for Sol 1 thin films. As can be seen from Figure 6, the exciton effect is detected for sol-gel undoped ZnO, ZnO:N and ZnO:F films, as the most pronounced exciton peak is found for ZnO:F 0.5 films annealed at 500 and 600 °C. The presence of the excitonic peak indicates that ZnO doped films have high structural quality, as the exciton absorption is related to film quality [53].

Table 2 gives the average transmittance and reflectance values of the studied sol-gel films (estimated for the wavelengths from 450 to 750 nm). The optical data clearly states that the transparency of ZnO:N:F films, obtained from Sol 1, is better than undoped ZnO films. ZnO:N:F films (Sol 2) reveal a deterioration of the film transparency. The fluorine doped ZnO films manifest the best transmittance values, reaching 91%. The excitonic formation and the good film transparency makes sol-gel doped ZnO films attractive for application in functional optical devices [54]. It must be noted that sol-gel spin coating deposition is a facile and flexible method for obtaining single and doped metal oxide films, characterized with smoothness and good optical properties.

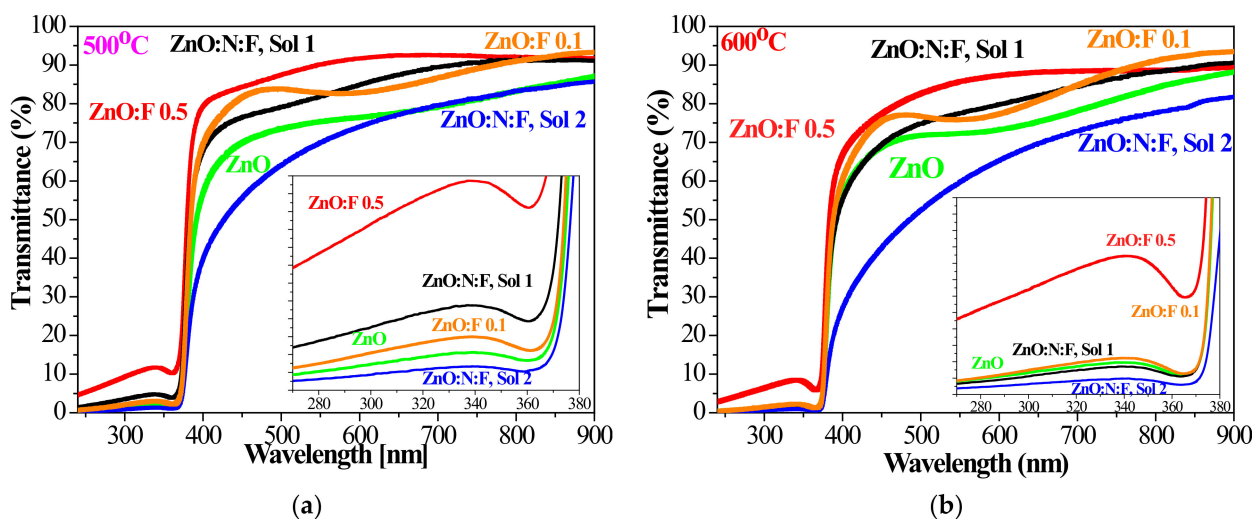


Figure 7. Comparison of the transmittance spectra of ZnO, ZnO:F and ZnO:N:F films, annealed at (a) 500 and (b) 600 °C in the spectral region 280–900 nm. The inset figures show the excitonic feature of the studied films.

Table 2. The average values of transmittance and reflectance of the studied sol-gel films, determined for the visible spectral range 450–750 nm. The average transmittance of bare quartz substrate is 93.53%.

Material	300 °C		400 °C		500 °C		600 °C	
	T _{average}	R _{average}						
ZnO	80.60	9.00	82.57	8.39	78.90	9.78	77.90	12.60
ZnO:F 0.1					86.74	8.64	83.60	11.13
ZnO:F 0.5					90.98	7.74	86.89	10.47
ZnO:N:F, Sol 1	84.75	8.12	88.18	6.40	86.65	8.25	82.62	7.88
ZnO:N:F, Sol 2	76.27	4.46	74.89	3.93	76.12	3.93	68.42	4.10

The estimated optical band gap (E_g) values are given in Figure 8. It can be observed that there is a narrowing of the optical band gap with the increasing of the annealing temperatures.

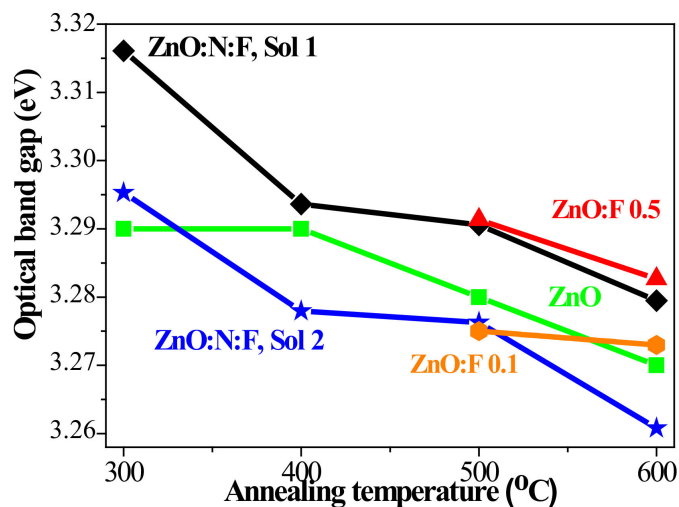


Figure 8. Optical band gap values of ZnO, ZnO:F and ZnO:N:F films, annealed at different temperatures.

It is known that optical band gap narrowing can be caused by defects and greater crystallite sizes [55]. The optical band gap (E_g) of ZnO:N:F films (Sol 1) is wider compared to

the undoped films. The E_g of ZnO:N:F films (Sol 1) has very close values to those of ZnO:F films. On the other hand, ZnO:N:F films (Sol 2) possess the lowest E_g values except for the value of 300 °C annealed samples. It was previously reported that F doping induces the widening of the optical band gap of the sol-gel ZnO films [35,56]. The increase of the energy gap values of ZnO films with the increase of the fluorine concentration can be attributed to the well-known Burstein–Möss effect. At the same time, it has been reported that the optical band gap is reduced with nitrogen incorporation in the ZnO structure [57]. It can be concluded that the widening of E_g is due to fluorine doping and nitrogen incorporation in ZnO results in the narrowing of optical band gaps. The crystallite size effect can also be considered, as it was determined that ZnO:N:F films (Sol 2) have the smallest crystallites (see Table 1). The obtained optical band gaps of sol-gel ZnO and doped ZnO films are in the range of the reported values [8,15,16,19,35,57].

3.4. FESEM Microscopy-Film Surface Morphology

The morphology of ZnO based films was examined by the FESEM technique and the recorded images are shown in Figures 9–11. The sol-gel thin films (ZnO, ZnO:N, ZnO:F and ZnO:N:F) were deposited on Si substrates and annealed at 600 °C in air. Our previous studies on ZnO-based films [31,33] reveal that the sol-gel undoped ZnO film, annealed at 600 °C, possesses a wrinkle-type network surface and a porous structure. Similar wrinkle morphology is often reported for ZnO and doped ZnO films, deposited by sol-gel technology [58,59]. The wrinkle formation of sol-gel films can be provoked by: (1) an increase in volumetric stress in the films and evaporation of the solvent [60], (2) a lack of hydroxyl (or alkoxy) groups from the sols during thermal treatments of the layers [61], (3) the release of mechanical stresses developed during densification and heat treatment of the films [62], (4) the difference between the thermal expansion coefficients of the substrate and film, and/or (5) volume reduction upon crystallization and film thickness [62]. The FTIR study shows that sol-gel ZnO films exhibit weak and broad absorption bands (3190–3600 cm^{-1}), related to the presence of hydroxyl groups after 300 °C annealing, and they vanished almost completely after the higher annealing treatments (400, 500 and 600 °C) [31,33]. Thus, this can contribute to wrinkle formation. In order to check, the other assumption, the microstrain can be estimated from XRD data:

$$\varepsilon = \frac{\beta \cos \theta}{4} \quad (4)$$

where β is the FWHM with respect to the (002) peak and θ is 002 peak position. The obtained microstrain values are given in Table 3.

The micro-strain values began to decrease with the doping as the ZnO:N film shows a closer strain to that of undoped ZnO. Nitrogen incorporation affects the ZnO morphology, but the wrinkle structure is still preserved (Figure 9). The smallest magnification Figure 9a shows that ZnO and ZnO:N films have wrinkle type morphologies. The FESEM imaging results, reported in Figure 9b,c, highlight the noticeable difference of the film morphology of these two materials: ZnO film exhibits a porous structure constituted by a wrinkle network with irregular grains extending over the entire surface of the layer. These grains differ in size and shape. Meanwhile, ZnO:N film also manifests a wrinkle formation, but the film has a denser structure and wider fiber-like stripes (wrinkles). The morphology of ZnO:N film is induced by hydroxyl groups and by the microstrain in its structure.

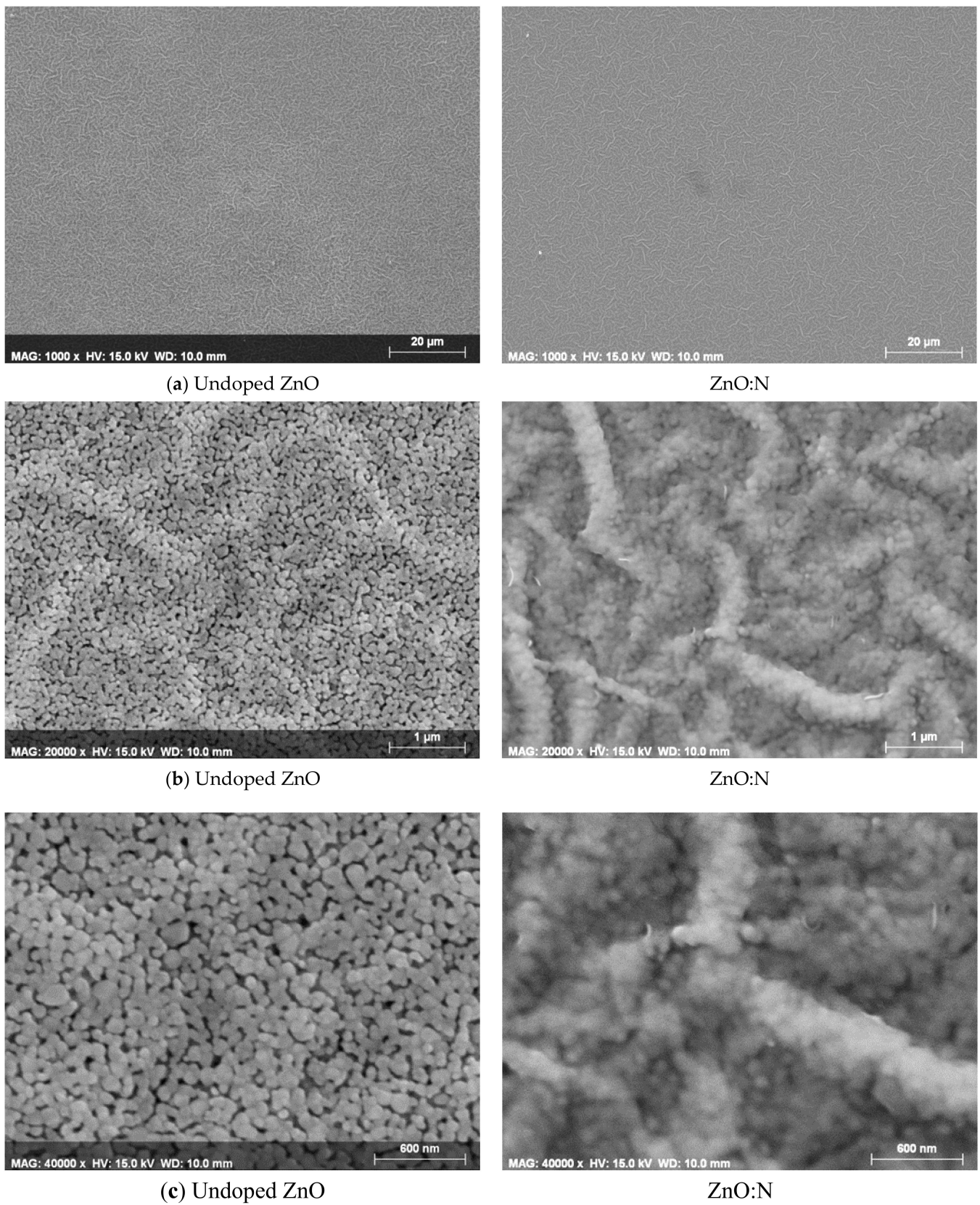
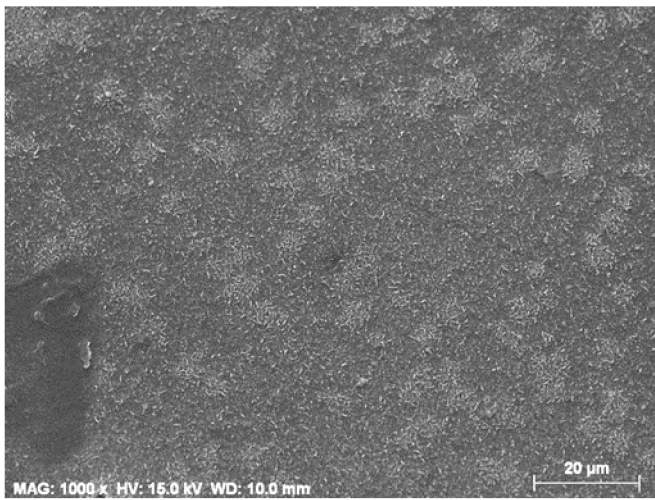
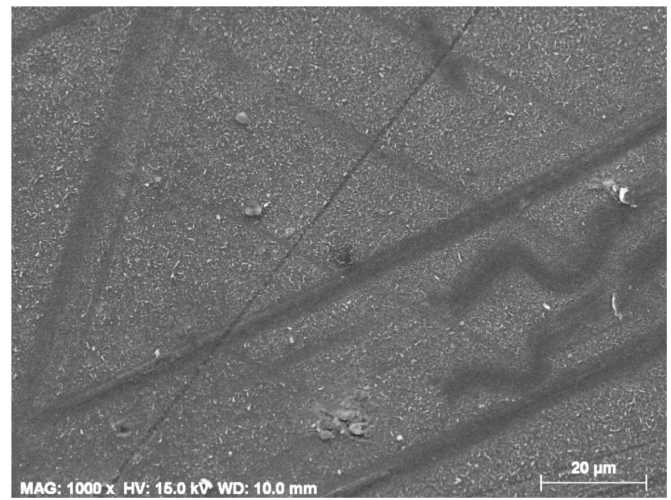


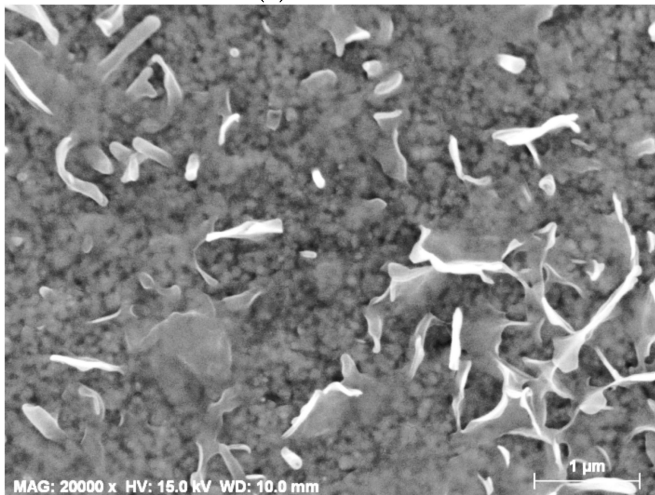
Figure 9. FESEM micrographs of (a) ZnO and ZnO:N films at magnification 1000, (b) ZnO and ZnO:N films at magnification 20,000 and (c) ZnO and ZnO:N films at magnification 40,000. The films are annealed at 600 °C.



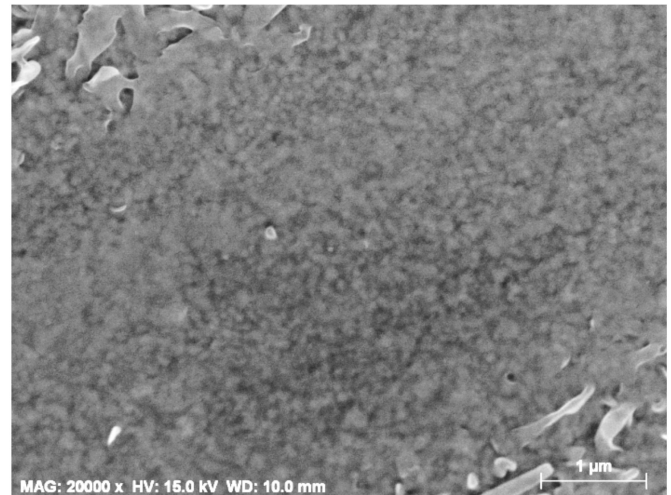
(a) ZnO:F 0.1



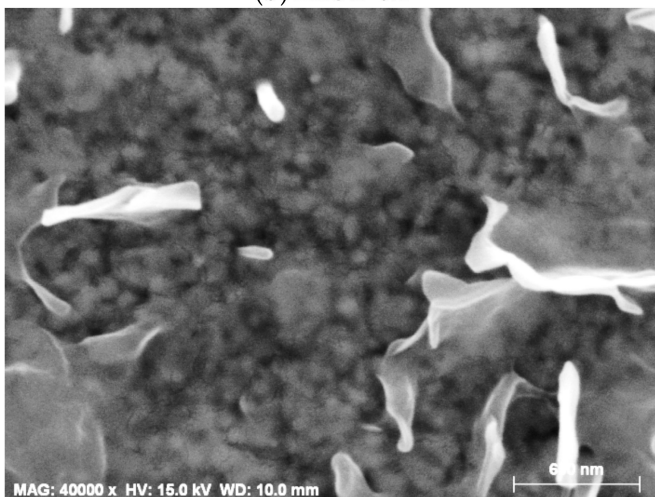
ZnO:F 0.5



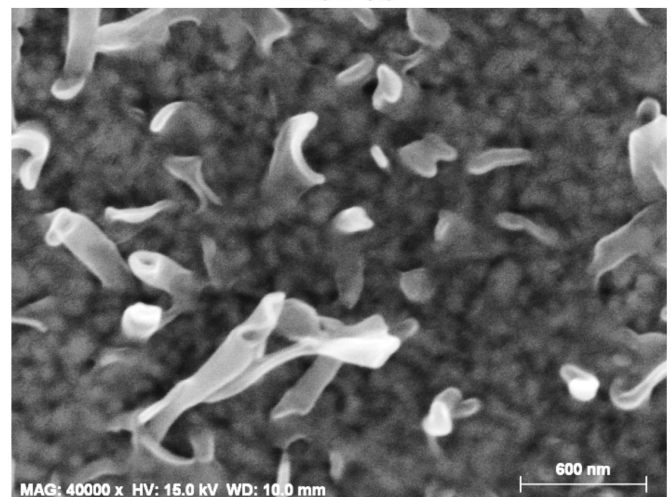
(b) ZnO:F 0.1



ZnO:F 0.5



(c) ZnO:F 0.1



ZnO:F 0.5

Figure 10. Cont.

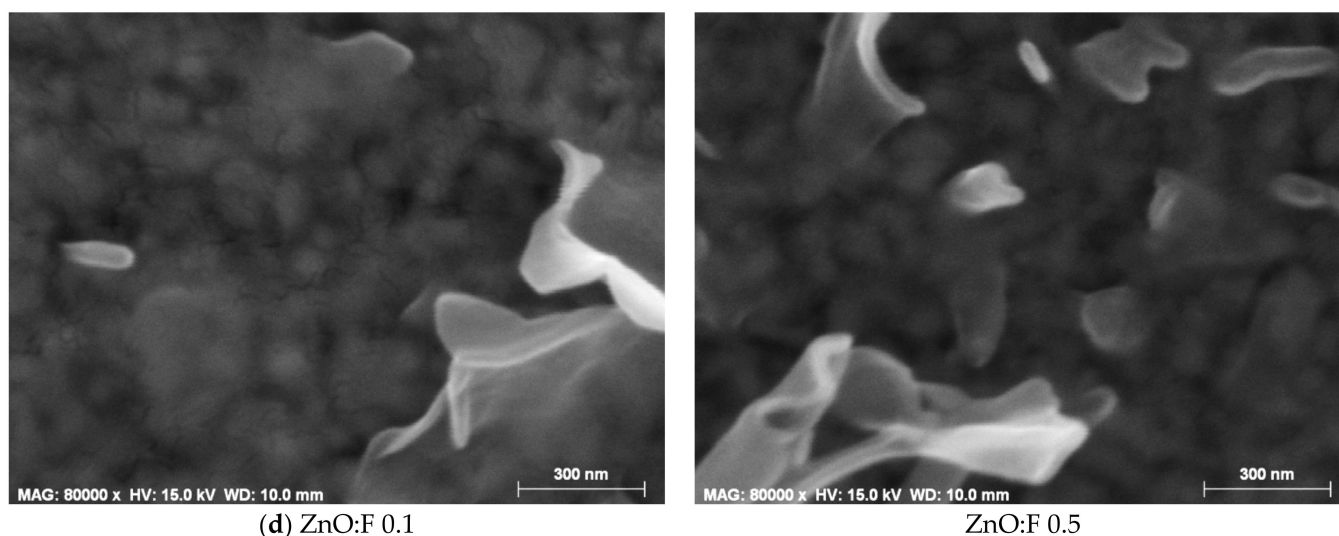


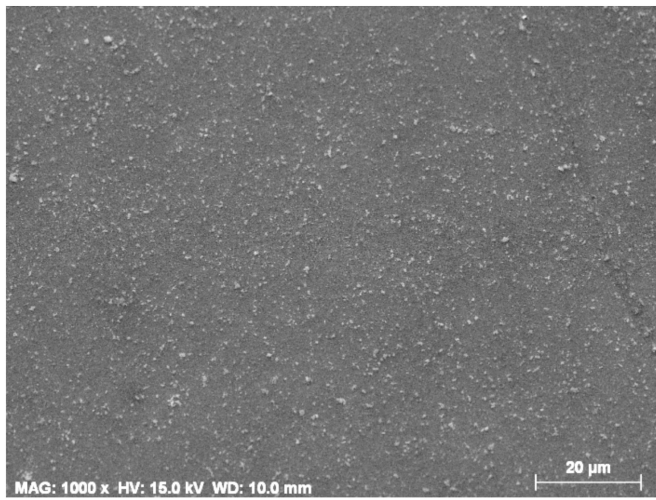
Figure 10. FESEM micrographs of (a) ZnO:F 0.1 and ZnO:F 0.5 films at magnification 1000, (b) ZnO:F 0.1 and ZnO:F 0.5 films at magnification 20,000, (c) ZnO:F 0.1 and ZnO:F 0.5 films at magnification 40,000 and (d) ZnO:F 0.1 and ZnO:F 0.5 films at magnification 80,000. The fluorine-doped ZnO films are thermally treated at 600 °C.

Table 3. Microstrain values, estimated for sol-gel ZnO and doped ZnO films.

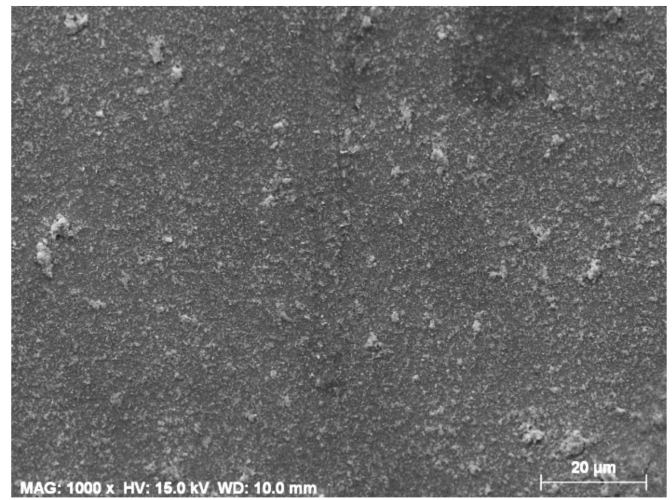
	ZnO	ZnO:F 0.1	ZnO:F 0.5	ZnO:N	ZnO:N:F, Sol 1	ZnO:N:F, Sol 2
ϵ	1.20099	0.85441	0.95776	1.19558	1.12218	1.30293

The grains of the ZnO:N surface are with spherical shapes and closely gathered together. The wrinkle width of ZnO varies in the range of 270–440 nm, while after nitrogen doping, the width is changed and it is between 400–480 nm.

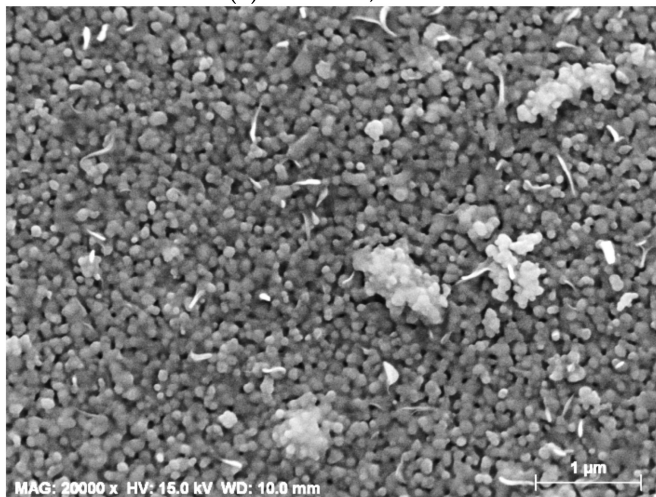
The fluorine doping in ZnO thin films strongly affected their surface morphology, as can be observed from Figure 10a. An FTIR study manifests that ZnO:F films have no absorption above 3000 cm^{-1} , related to OH vibrations. But as can be seen from Table 3, these films are the most relaxed, as their microstrain values are the lowest. As a result, the wrinkles disappear with fluorine doping. The formation of a granular nanometric phase together with microflakes and plate-like features are grown in perpendicular direction to the substrate surface (Figure 10b–d). The effect is dependent on the fluorine concentrations. Interestingly, the higher doping content induces smoother surface and, respectively, ZnO:F 0.5 films possess higher transparency (see Table 2). The morphology of ZnO:F 0.1 consists of grains and flakes, and this film shows a denser structure. The grains of ZnO:F 0.1 films differ in sizes ranging from 20 to 80 nm. Bigger clusters are observed, but they consist of smaller spherical grains. ZnO:F 0.5 films show some flakes and nanometric tubes, and the grains are greater than those of ZnO:F 0.1, in alignment with the XRD results (Table 1). The fluorine doped ZnO films reveal dense morphology. Fluorine influences the ZnO surface morphology as it urges denser films and modifies the wrinkle network in the granular structure with specific features.



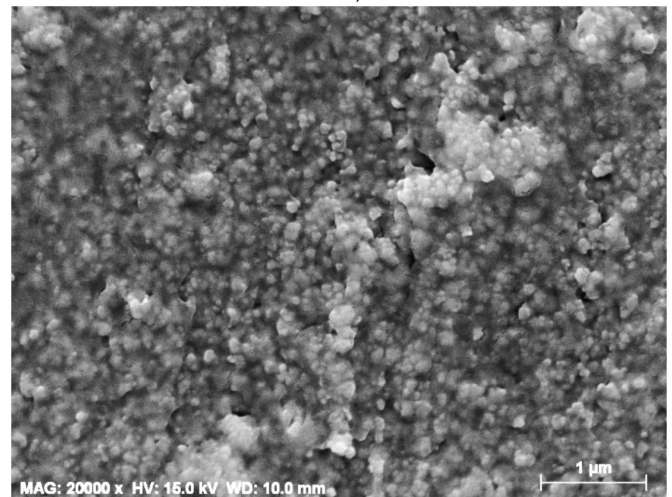
(a) ZnO:N:F, Sol 1



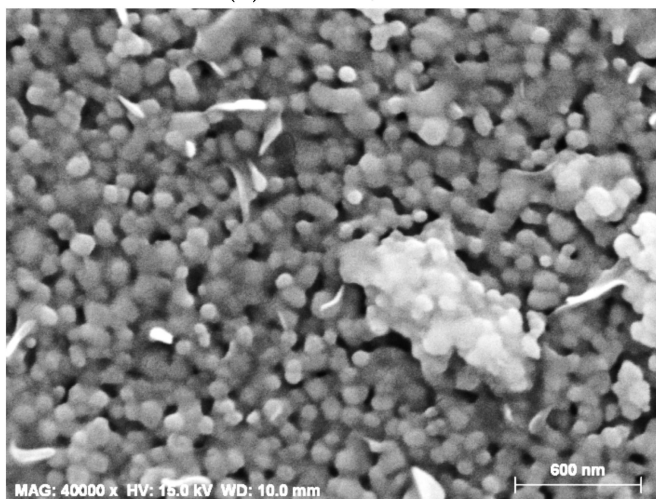
ZnO:N:F, Sol 2



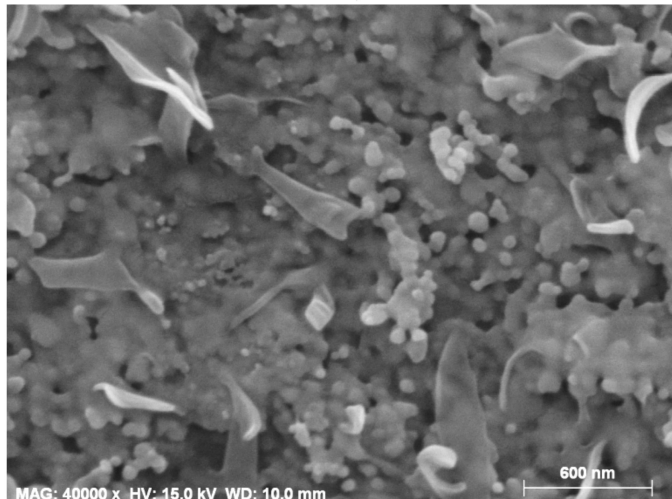
(b) ZnO:N:F, Sol 1



ZnO:N:F, Sol 2



(c) ZnO:N:F, Sol 1



ZnO:N:F, Sol 2

Figure 11. Cont.

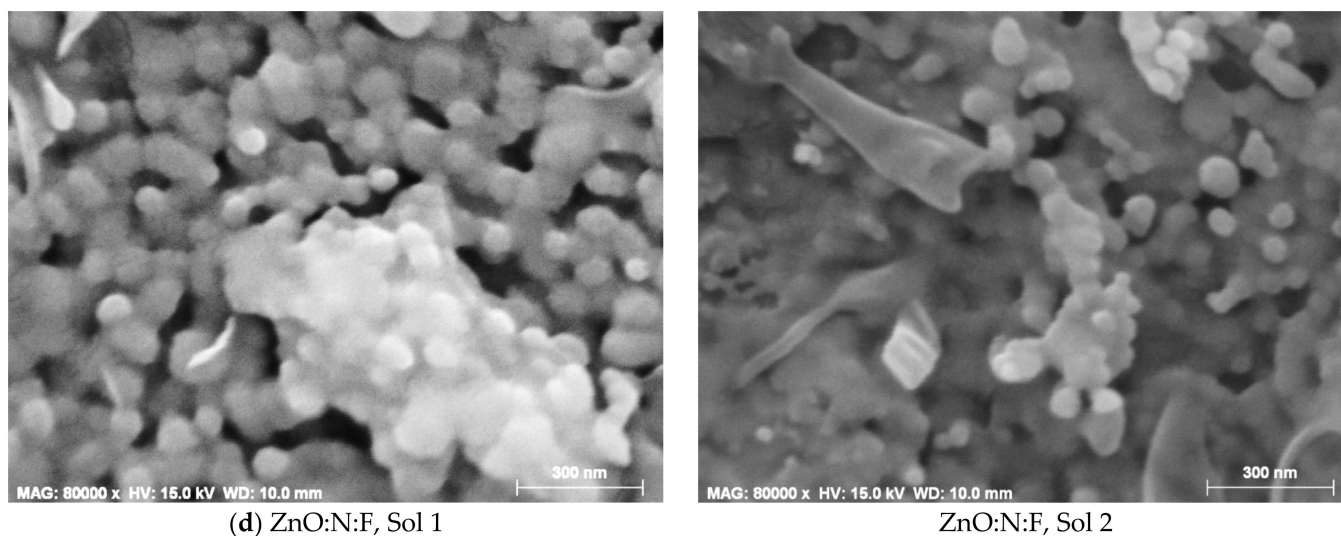


Figure 11. FESEM micrographs of (a) ZnO:N:F, sol 1 and ZnO:N:F sol 2 films at magnification 1000, (b) ZnO:N:F, sol 1 and ZnO:N:F sol 2 at magnification 20,000, (c) ZnO:N:F, sol 1 and ZnO:N:F sol 2 at magnification 40,000 and (d) ZnO:N:F, sol 1 and ZnO:N:F sol 2 at magnification 80,000. The N, F co-doped ZnO films are annealed at 600 °C.

The micrographs at different magnifications of the sol-gel ZnO:N:F films, obtained from Sol 1 and Sol 2, are given in Figure 11. It is clearly seen that there are no wrinkles or fiber-like features (Figure 11a,b, magnification 1000 and 20,000). These results indicate that the co-doping with nitrogen and fluorine affects the film morphology by transforming the wrinkle network into the grained structure. It can be noted (Figure 11b) that Sol 1 film reveals a smoother surface. A closer look (Figure 11c, magnification 40,000) reveals clear differences in the film morphology: ZnO:N:F film (Sol 1) has a grained structure with some pores and agglomerates and ZnO:N:F film (Sol 2) exhibits a rather rough surface and a denser structure with grains with wide size distribution as well as irregular flakes. ZnO:N:F film (deposited from Sol 1) shows a steadier surface as randomly and rarely distributed bigger clusters and some formations like flakes. These features are suggested to be due to the influence of F doping. The closest look of ZnO:N:F films (Figure 10d, 80,000 magnification) demonstrates that the grains of ZnO:N:F film (Sol 1) are a spherical type with different sizes (in the wide range of 30–90 nm), in which the presence of the pores and clusters can clearly be observed. ZnO:N:F film, obtained from Sol 2, possesses rougher surface with multisized grains that are gathered together with indefinite boundaries. The optical characterization displays that ZnO:N:F film (Sol 1), treated at 600 °C possesses a high transparency of 82.6% (average transmittance 450–800 nm) with the corresponding reflectance of 7.88%. Meanwhile, ZnO:N:F film (Sol 2) has lower transmittance (68.42%) and a lower reflectance of 4.0%. The rougher film surface provokes diminished transparency and probably greater light scattering.

An FESEM study proves that single doping with nitrogen results in denser and bigger wrinkles compared to undoped ZnO film. The fluorine incorporation induces a significant modification of ZnO film morphology, as the granular structure is seen together with flakes, plate and nanotube-like features. The higher F doping concentration improves the film surface uniformity. The co-doping with N and F reflects on the films as there is no wrinkle-type formation. The film morphology can explain the differences in the film transparency of the sol-gel ZnO and doped ZnO films.

4. Conclusions

Transparent and smooth ZnO, single and dual (F, N) doped ZnO films were successfully deposited on Si and quartz substrates by the sol-gel spin coating method. The influences of the doping elements and high temperature annealings on the crystal structure,

optical properties and morphology were investigated. An XRD analysis showed that ZnO, ZnO:N, ZnO:F and ZnO:N:F films crystallized in a hexagonal wurtzite structure. The co-doping with N and F resulted in smaller crystallite sizes compared to the single F and N doped ZnO films. Single nitrogen and fluorine doping provoked the growth of greater crystallites. The texture coefficients of the crystal planes of 100, 002 and 101 were determined and discussed. The grain growth orientation was changed upon fluorine and nitrogen incorporation. An FTIR study confirmed XRD conclusions that the films maintained the wurtzite ZnO structure. The main absorption band Zn-O in the spectra of ZnO and ZnO:F films were at 395 cm^{-1} , and N doping moved it to 407 cm^{-1} . ZnO:N:F films exhibited IR absorption at 405 cm^{-1} .

The transparency of ZnO:N:F films, obtained from Sol 1, was improved with respect to undoped ZnO films with a transparency above 82% and a reflectance below 8.5% in the visible spectral range. ZnO:F films had the highest transmittance of 91% after thermal treatment at $500\text{ }^{\circ}\text{C}$. The optical band gaps of ZnO:N:F films, obtained from Sol 1, varied from 3.32 to 3.28 eV with the increase in the annealing temperature. They were greater from the corresponding values of undoped ZnO films (3.29–3.27 eV). On the other hand, ZnO:N:F films, Sol 2 revealed lower values compared to ZnO after treatment at 400, 500 and $600\text{ }^{\circ}\text{C}$, and they ranged from 3.28 to 3.26 eV. An FESEM study revealed that nitrogen doping in ZnO films produced denser and bigger wrinkles compared to undoped film. The fluorine incorporation modified ZnO film morphology into a granular-type structure with the appearance of flakes and plate like features. The N, F co-doping resulted in surface morphologies with spherical and irregular grains and a porous structure. The effect of co-doping in ZnO was the modification of wrinkle-type structure.

Co-doping ZnO films with N and F modified the structural, optical and morphological properties. The proposed sol-gel method is facile and applicable for depositing nanostructured doped thin films. The studied ZnO based films are suitable candidates for application in optoelectronic devices.

Author Contributions: T.I.; Investigation, formal analysis, writing—original draft preparation, writing—review and editing; A.H.; Methodology, Investigation, Validation; T.K.; Investigation; B.V.; Investigation; R.C.; Investigation. All authors have read and agreed to the published version of the manuscript.

Funding: This research received no external funding.

Institutional Review Board Statement: Not applicable.

Informed Consent Statement: Not applicable.

Data Availability Statement: The data are not publicly available.

Conflicts of Interest: The authors declare that they have no conflict of interest.

References

1. Znaidi, L. Sol-gel-deposited ZnO thin films: A review. *Mater. Sci. Eng. B* **2010**, *174*, 18–30. [[CrossRef](#)]
2. Jin, Y.; Zhang, N.; Zhang, B. Fabrication of p-Type ZnO:N Films by Oxidizing Zn_3N_2 Films in Oxygen Plasma at Low Temperature. *Materials* **2017**, *10*, 236. [[CrossRef](#)] [[PubMed](#)]
3. Khalafi, T.; Buazar, F.; Ghanemi, K. Phycosynthesis and Enhanced Photocatalytic Activity of Zinc Oxide Nanoparticles Toward Organosulfur Pollutants. *Sci. Rep.* **2019**, *9*, 6866. [[CrossRef](#)] [[PubMed](#)]
4. Hussain, M.; Khan, A.; Nur, O.; Willander, M.; Broitman, E. The effect of oxygen-plasma treatment on the mechanical and piezoelectrical properties of ZnO nanorods. *Chem. Phys. Lett.* **2014**, *608*, 235–238. [[CrossRef](#)]
5. Tiwari, V.; Mishra, N.; Gadani, K.; Solanki, P.S.; Shah, N.A.; Tiwari, M. Mechanism of Anti-bacterial Activity of Zinc Oxide Nanoparticle Against Carbapenem-Resistant *Acinetobacter baumannii*. *Front. Microbiol.* **2018**, *9*, 1218. [[CrossRef](#)]
6. Levinson, L.; Philipp, H. Zinc oxide varistors—A review. *Am. Ceram. Soc. Bull.* **1986**, *65*, 639–646.
7. Djurišić, A.B.; Ng, A.M.C.; Chen, X. ZnO nanostructures for optoelectronics: Material properties and device applications. *Prog. Quantum Electron.* **2010**, *34*, 191–259. [[CrossRef](#)]
8. Sharmin, A.; Tabassum, S.; Bashar, M.S.; Mahmood, Z.H. Depositions and characterization of sol-gel processed Al-doped ZnO (AZO) as transparent conducting oxide (TCO) for solar cell application. *J. Theor. Appl. Phys.* **2019**, *13*, 123–132. [[CrossRef](#)]

9. Huang, H.Y.; Chiang, H.J.; Wu, C.Z.; Lin, Y.; Shen, Y.K. Analysis on Characteristics of ZnO Surface Acoustic Wave with and without Micro-Structures. *Micromachines* **2019**, *10*, 434. [[CrossRef](#)]
10. Jin, S.E.; Jin, H.E. Synthesis, Characterization, and Three-Dimensional Structure Generation of Zinc Oxide-Based Nanomedicine for Biomedical Applications. *Pharmaceutics* **2019**, *11*, 575. [[CrossRef](#)]
11. Yamamoto, O. Influence of particle size on the antibacterial activity of zinc oxide. *Int. J. Inorg. Mater.* **2001**, *3*, 643–646. [[CrossRef](#)]
12. Zhou, Z.; Zhang, Y.; Chen, X.; Li, S.; Zhao, Y.; Zhang, X. Innovative Wide-Spectrum Mg and Ga-Codoped ZnO Transparent Conductive Films Grown via Reactive Plasma Deposition for Si Heterojunction Solar Cells. *ACS Appl. Energy Mater.* **2020**, *3*, 1574–1584. [[CrossRef](#)]
13. Chen, S.; Warwick, M.E.A.; Binions, R. Effects of film thickness and thermal treatment on the structural and opto-electronic properties of Ga-doped ZnO films deposited by sol–gel method. *Sol. Energy Mater. Sol. Cells* **2015**, *137*, 202–209. [[CrossRef](#)]
14. Muhammad, A.; Hassan, Z.; Mohammad, S.M.; Rajamanickam, S. Enhanced sensitivity of low-cost fabricated fluorine doped ZnO metal semiconductor metal photodetector. *Opt. Mater.* **2021**, *122*, 111771. [[CrossRef](#)]
15. Liu, Y.; Li, Y.; Zeng, H. ZnO-Based Transparent Conductive Thin Films: Doping, Performance, and Processing. *J. Nanomat.* **2013**, *2013*, 196521. [[CrossRef](#)]
16. Podporska-Carroll, J.; Myles, A.; Quilty, B.; McCormack, D.E.; Fagan, R.; Hinder, S.J.; Dionysiou, D.D.; Pillai, S. Antibacterial properties of F-doped ZnO visible light photocatalyst. *J. Hazardous Mater.* **2015**, *324*, 39–47. [[CrossRef](#)]
17. Zhao, W.; Li, H.; Liu, Z.; Wang, D.; Liu, S. Controlled defects and enhanced electronic extraction in fluorine-incorporated zinc oxide for high-performance planar perovskite solar cells. *Sol. Energy Mater. Sol. Cells* **2018**, *182*, 263–271. [[CrossRef](#)]
18. Huang, Z.; Ruan, H.; Zhang, H.; Shi, D.; Li, W.; Qin, G.; Wu, F.; Fang, L.; Kong, C. Investigation on the p-type formation mechanism of nitrogen ion implanted ZnO thin films induced by rapid thermal annealing. *Opt. Mater. Express* **2019**, *9*, 3098–3108. [[CrossRef](#)]
19. Dhara, S.; Giri, P.K. Stable p-type conductivity and enhanced photoconductivity from nitrogen-doped annealed ZnO thin film. *Thin Solid Films* **2012**, *520*, 5000–5006. [[CrossRef](#)]
20. Yu, C.F.; Lin, T.J.; Sun, S.J.; Chou, H. Origin of ferromagnetism in nitrogen embedded ZnO:N thin films. *J. Phys. D Appl. Phys.* **2007**, *40*, 6497–6500. [[CrossRef](#)]
21. Ievtushenko, A.; Lashkarev, G.; Lazorenko, V.; Karpyna, V.; Sichkovskiy, V.; Kosyachenko, L.; Sklyarchuk, V.; Sklyarchuk, O.; Bosy, V.; Korzhinski, F.; et al. Ultraviolet Detectors Based on ZnO:N Thin Films with Different Contact Structures. *Acta Phys. Pol. A* **2008**, *114*, 1123–1129. [[CrossRef](#)]
22. Prasad, R.; Walke, P.S.; Bham, S.D. Structural and optical studies on flowerlike strontium doped zinc oxide synthesized by hydrothermal method. *Mater. Res. Express* **2019**, *6*, 1150b8. [[CrossRef](#)]
23. Lokhande, B.J.; Patil, P.S.; Uplane, M.D. Studies on structural, optical and electrical properties of boron doped zinc oxide films prepared by spray pyrolysis technique. *Phys. B Condens. Matter.* **2001**, *302–303*, 59–63. [[CrossRef](#)]
24. Ponja, S.D.; Sathasivam, S.; Parkin, I.P.; Carmalt, C.J. Highly conductive and transparent gallium doped zinc oxide thin films via chemical vapor deposition. *Sci. Rep.* **2020**, *10*, 638. [[CrossRef](#)] [[PubMed](#)]
25. Stamate, E. Spatially Resolved Optoelectronic Properties of Al-Doped Zinc Oxide Thin Films Deposited by Radio-Frequency Magnetron Plasma Sputtering Without Substrate Heating. *Nanomaterials* **2020**, *10*, 14. [[CrossRef](#)]
26. Hashmi, J.Z.; Siraj, K.; Latif, A.; Naseem, S.; Murray, M.; Jose, G. The role of samarium incorporated structural defects in ZnO thin films prepared by femtosecond pulsed laser deposition. *J. Alloys Comp.* **2019**, *800*, 191–197. [[CrossRef](#)]
27. Ilican, S.; Caglar, M.; Aksoy, S.; Caglar, Y. XPS Studies of Electrodeposited Grown F-Doped ZnO Rods and Electrical Properties of p-Si/n-FZN Heterojunctions. *J. Nanomater.* **2016**, *2016*, 6729032. [[CrossRef](#)]
28. Najafi, A.; Sharifi, F.; Mesgari-Abbasi, S.; Khalaj, G. Influence of pH and temperature parameters on the sol-gel synthesis process of meso porous ZrC nanopowder. *Ceram. Int.* **2022**, *48*, 26725–26731. [[CrossRef](#)]
29. Tang, G.; Liu, H.; Zhang, W. The Variation of Optical Band Gap for ZnO:In Films Prepared by Sol-Gel Technique. *Adv. Mater. Sci. Engin.* **2013**, *2013*, 348601. [[CrossRef](#)]
30. Kamoun, O.; Gassoumi, A.; Shkir, M.; Gorji, N.E.; Turki-Kamoun, N. Synthesis and Characterization of Highly Photocatalytic Active Ce and Cu Co-Doped Novel Spray Pyrolysis Developed MoO₃ Films for Photocatalytic Degradation of Eosin-Y Dye. *Coatings* **2022**, *12*, 823. [[CrossRef](#)]
31. Ivanova, T.; Harizanova, A.; Koutzarova, T.; Vertruyen, B.; Stefanov, B. Structural and morphological characterization of sol-gel ZnO:Ga films: Effect of annealing temperatures. *Thin Solid Films* **2018**, *646*, 132–142. [[CrossRef](#)]
32. Ivanova, T.; Harizanova, A.; Koutzarova, T.; Vertruyen, B. Optical and structural properties of sol-gel derived ZnO:F thin films. *AIP Conf. Proc.* **2019**, *2075*, 140005.
33. Ivanova, T.; Harizanova, A.; Koutzarova, T.; Vertruyen, B.; Closset, R. Structural and optical characterization of nitrogen and gallium co-doped ZnO thin films, deposited by sol-gel method. *J. Mol. Struct.* **2020**, *1206*, 127773. [[CrossRef](#)]
34. Ahmad, S.; Kharkwal, M.; Govind; Nagarajan, R. Application of KZnF₃ as a Single Source Precursor for the Synthesis of Nanocrystals of ZnO₂:F and ZnO:F; Synthesis, Characterization, Optical, and Photocatalytic Properties. *J. Phys. Chem. C* **2011**, *115*, 10131–10139. [[CrossRef](#)]
35. Widayastuti, E.; Hsu, J.L.; Lee, Y.C. Insight on Photocatalytic and Photoinduced Antimicrobial Properties of ZnO Thin Films Deposited by HiPIMS through Thermal Oxidation. *Nanomaterials* **2022**, *12*, 463. [[CrossRef](#)]

36. Kumari, R.; Sahai, A.; Goswami, N. Effect of nitrogen doping on structural and optical properties of ZnO nanoparticles. *Prog. Natural Sci. Mater. Inter.* **2015**, *25*, 300–309. [[CrossRef](#)]
37. Hariwal, R.V.; Malik, H.K.; Negi, A.; Kandasami, A. Controlling room temperature ferromagnetism and band gap in ZnO nanostructured thin films by varying angle of implantation. *RCA Adv.* **2018**, *8*, 6278–6287. [[CrossRef](#)]
38. Morkoc, H.; Ozgur, U. *Zinc Oxide: Fundamentals Materials and Device Technology*; Wiley: Weinheim, Germany, 2009; pp. 1–14.
39. Kim, K.K.; Kim, H.S.; Hwang, D.K.; Lim, J.H.; Park, S.J. Realization of p-type ZnO thin films via phosphorus doping and thermal activation of the dopant. *Appl. Phys. Lett.* **2003**, *83*, 63–65. [[CrossRef](#)]
40. Malek, M.F.; Mamat, M.H.; Sahdan, M.Z.; Zahidi, M.M.; Khusaimi, Z.; Mahmood, M.R. Influence of various sol concentrations on stress/strain and properties of ZnO thin films synthesised by sol-gel technique. *Thin Solid Films* **2013**, *527*, 102–109. [[CrossRef](#)]
41. Znaidi, L.; Touam, T.; Vrel, D.; Souded, N.; Yahia, S.B.; Brinza, O.; Fischer, A.; Boudrioua, A. AZO Thin Films by Sol-Gel Process for Integrated Optics. *Coatings* **2013**, *3*, 126–139. [[CrossRef](#)]
42. Liton, M.N.H.; Khan, M.K.R.; Rahman, M.M.; Islam, M.M. Effect of N and Cu Doping on Structure, Surface Morphology and Photoluminescence Properties of ZnO Thin Films. *J. Sci. Res.* **2015**, *7*, 23–32. [[CrossRef](#)]
43. Petrovic, Z.; Ristic, M.; Music, S. Development of ZnO microstructures produced by rapid hydrolysis of zinc acetylacetonate. *Ceram. Int.* **2014**, *40*, 10953–10959. [[CrossRef](#)]
44. Marikutsa, A.; Romyantsev, M.; Gaskov, A.; Batuk, M.; Hadermann, J.; Sarmadian, N.; Saniz, R.; Portoens, B.; Lamoen, P. Effect of Zinc Oxide Modification by Indium Oxide on Microstructure, Adsorbed Surface Species, and Sensitivity to CO. *Front. Mater.* **2019**, *6*, 43. [[CrossRef](#)]
45. Zerdali, M.; Hamzaoui, S.; Teherani, F.H.; Rogers, D. Growth of ZnO thin film on SiO₂/Si substrate by pulsed laser deposition and study of their physical properties. *Mater. Lett.* **2006**, *60*, 504–508. [[CrossRef](#)]
46. Sudrajat, H.; Babel, S. A novel visible light active N-doped ZnO for photocatalytic degradation of dyes. *J. Water Process Eng.* **2017**, *16*, 309–318. [[CrossRef](#)]
47. Javayarambabu, N.; Kumari, B.S.; Rao, K.V.; Prabhu, Y.T. Beneficial role of zinc oxide nanoparticles on green crop production. *Int. J. Multidiscip. Adv. Res. Trends* **2015**, *II*, 273–282.
48. Abinaya, C.; Marikkannan, M.; Manikandan, M.; Mayandi, J.; Suresh, P.; Shanmugaiah, V.; Ekstrum, C.; Pearce, J.M. Structural and optical characterization and efficacy of hydrothermal synthesized Cu and Ag doped zinc oxide nanoplate bactericides. *Mater. Chem. Phys.* **2016**, *184*, 172–182. [[CrossRef](#)]
49. Xiong, G.; Pal, U.; Umapada, J.; Serrano, J.; Ucer, K.B.; Williams, R.T. Photoluminescence and FTIR study of ZnO nanoparticles: The impurity and defect perspective. *Phys. Status Solidi C* **2006**, *3*, 3577–3581. [[CrossRef](#)]
50. Keyes, B.M.; Gedvilas, L.M.; Li, X.; Coutts, T.J. Infrared spectroscopy of polycrystalline ZnO and ZnO:N thin films. *J. Cryst. Growth* **2005**, *281*, 297–302. [[CrossRef](#)]
51. Cao, Y.; Yu, M.; Qi, S.; Wang, T.; Huang, S.; Hu, S.; Xu, M.; Yan, S. Formation and evolution of orientation-specific CO₂ chains on nonpolar ZnO (10 $\bar{1}$ 0) surfaces. *Sci. Rep.* **2017**, *7*, 43442. [[CrossRef](#)]
52. Nandakumar, N.; Dielissen, B.; Garcia-Alonso, D.; Liu, Z.; Gortzen, R.; Kessels, W.M.M.E.; Hoex, B. Resistive Intrinsic ZnO Films Deposited by Ultrafast Spatial ALD for PV Applications. *IEEE J. Photovolt.* **2015**, *5*, 1462–1469. [[CrossRef](#)]
53. Rai, R.C.; Guminiak, M.; Wilser, S.; Cai, B.; Nakarm, M.L. Elevated temperature dependence of energy band gap of ZnO thin films grown by e-beam deposition. *J. Appl. Phys.* **2012**, *111*, 073511. [[CrossRef](#)]
54. Pilz, J.; Perrotta, A.; Leising, G.; Coclite, A.M. ZnO Thin Films Grown by Plasma-Enhanced Atomic Layer Deposition: Material Properties Within and Outside the “Atomic Layer Deposition Window”. *Phys. Status Solidi A* **2020**, *270*, 1900256. [[CrossRef](#)]
55. Mostafa, N.Y.; Heiba, Z.K.; Ibrahim, M.M. Structure and optical properties of ZnO produced from microwave hydrothermal hydrolysis of tris(ethylenediamine)zinc nitrate complex. *J. Mol. Struct.* **2015**, *1079*, 480–485. [[CrossRef](#)]
56. Alkhayalt, A.H.O.; Hussain, S.K. Fluorine dopant concentration effect on the structural and optical properties of spray deposited nanocrystalline ZnO thin films. *Surf. Interfaces* **2017**, *8*, 176–181. [[CrossRef](#)]
57. Tiron, V.; Velicu, I.L.; Stanescu, D.; Magnan, H.; Sirghi, L. High visible light photocatalytic activity of nitrogen-doped ZnO thin films deposited by HiPIMS. *Surf. Coat. Technol.* **2017**, *324*, 594–600. [[CrossRef](#)]
58. Li, X.; Zhu, X.; Yang, D. Enhanced luminescent performance with surface wrinkled Al-doped ZnO films. *J. Mater. Sci. Mater. Electron.* **2020**, *31*, 6304–6312. [[CrossRef](#)]
59. Rana, V.S.; Rajput, J.K.; Pathaka, T.K.; Purohit, L.P. Cu sputtered Cu/ZnO Schottky diodes on fluorine doped tin oxide substrate for optoelectronic applications. *Thin Solid Films* **2019**, *679*, 79–85. [[CrossRef](#)]
60. Navin, K.; Kurchania, R. Structural, morphological and optical studies of ripple-structured ZnO thin films. *Appl. Phys. A* **2015**, *121*, 1155–1161. [[CrossRef](#)]
61. Bu, I.Y.Y. Self-assembled, wrinkled zinc oxide for enhanced solar cell performances. *Mater. Lett.* **2014**, *122*, 55–57. [[CrossRef](#)]
62. Miller, J.B.; Hsie, H.J.; Howard, B.H.; Broitman, E. Microstructural evolution of sol-gel derived ZnO thin films. *Thin Solid Films* **2010**, *518*, 6792–6798. [[CrossRef](#)]